

Admu Yebi¹

Mem. ASME
Clemson University—International
Center for Automotive Research,
4 Research Dr.,
Greenville, SC 29607
e-mail: ayebi@clemson.edu

Beshah Ayalew

Associate Professor
Mem. ASME
Clemson University—International Center for
Automotive Research,
4 Research Dr., CGEC342,
Greenville, SC 29607
e-mail: beshah@clemson.edu

Srikanth Pilla

Assistant Professor
Clemson University—International Center
for Automotive Research,
4 Research Dr., CGEC340,
Greenville, SC 29607
e-mail: spilla@clemson.edu

Xiaoyan Yu

Clemson University—International Center
for Automotive Research,
4 Research Dr.,
Greenville, SC 29607
e-mail: xyu4@clemson.edu

Model-Based Robust Optimal Control for Layer-By-Layer Ultraviolet Processing of Composite Laminates

This paper first discusses some experimental verification of proposed ultraviolet (UV) radiation curing process models and then it outlines a robust process optimization and control scheme for layer-by-layer UV processing of a thick composite laminate. The experiments include UV transmission, cure kinetics, and in situ temperature measurements for UV curing of a one-dimensional (1D) composite material sample. The validated models are used to motivate how optimizing the layer-by-layer curing process can help address the challenge of maintaining through-cure due to the in-domain attenuation of the UV input during thick-part fabrication. The key insight offered is to model the layer-by-layer deposition and curing process as a multi-mode hybrid dynamic system with a growing spatial domain, where the interlayer hold times and the UV intensity at each layer addition can be taken as the augmented control variables to be selected optimally. Specifically, the control input is set to have feed forward and output feedback components, which act on the UV intensity at each layer and are constructed to track a reference surface temperature trajectory. The feedback gains at each layer addition are designed by posing a robust optimization problem that penalizes the sensitivity of the objective function to process uncertainties. It is illustrated using simulation analyses that augmented control with robust optimal static feedback of UV intensity at each layer and nominal optimization of the interlayer hold times gives very close tracking of a desired final cure level distribution in the presence of parametric uncertainty. [DOI: 10.1115/1.4034782]

Keywords: hybrid modeling, layer-by-layer manufacturing, robust optimal control of hybrid systems, UV curing process, composite manufacturing

1 Introduction

Composite materials are attractive for many structural light weighting applications such as automotive and aerospace. While raw material costs continue to decline [1], the time and costs associated with the complexities of manufacturing processes for composites are still a challenge. For example, the dominant processes for curing composites involve the use of autoclave facilities (thermal curing). These typically feature high capital costs, high-energy consumption, and long processing times [2,3]. To overcome this challenge, radiation-based technology such as UV processing of composite laminates has been considered as a viable out of autoclave (OOA) alternative because of its energy efficiency and accelerated processing time [4,5]. As an example, a comparative study in Ref. [4] showed that UV curing for a fiberglass composite only takes 10 mins to produce a product of acceptable quality while the thermal counterpart takes over 4 hrs while involving higher level of styrene emission (four times higher).

Despite these advantages, adoption of UV technology is limited to curing of thin sections because of the significant attenuation of UV radiation as it passes through thick target materials [6]. This could be compensated by feedback control design. Such feedback compensation [7] only yields good results for parts of limited thickness (<5 mm). To overcome this attenuation or cure penetration problem for relatively large thickness, an approach of layer-by-layer deposition and curing of composite laminates is often adopted. Duan et al. [2] conducted an experiment that

demonstrated the feasibility of layer-by-layer curing approach, which resulted in improved mechanical properties in the end product. In another work, Wang [8] conducted model-based investigations of in situ UV-laser curing of polymer composites using the filament winding method that aims to cure relatively large thicknesses by applying the UV-laser on the tow while it is being wound on the mandrel. However, still some challenges remain such as differing material shrinkage and thermal stresses between layers due to cure level and temperature gradients across layers that lead to distortion of the end product [9].

To overcome these challenges, in our previous work [10], we proposed a stepped-concurrent layering and curing (SCC) processes, where new layers are added before previous ones cure completely in such a way that there is an effective reduction of cure level deviation and thermal stress in all layers. To further exploit the potential of the SCC approach, we then developed a systematic model-based dynamic optimization scheme by modeling the layering process a hybrid dynamic system. In SCC, the successive addition of each layer changes both the spatial domains and the initial conditions of the physical processes. As a result, the SCC process is naturally regarded as a multimode hybrid system with a predefined mode sequence and a growing spatial domain (which leads to a growing state dimension in discretized form). In Ref. [10], we motivated the need of optimal interlayer hold times for SCC and developed an optimization algorithm to compute this optimal hold times by treating them as the control inputs. Later in Ref. [11], we studied the effect of the augmented optimization of both layer-by-layer UV input intensity and interlayer hold times as the control variables. Both of our previous works only dealt with model-based optimizations that consider nominal process parameters. However, uncertain model parameters related to cure kinetics such as constants related to reaction order and activation

¹Corresponding author.

Contributed by the Dynamic Systems Division of ASME for publication in the JOURNAL OF DYNAMIC SYSTEMS, MEASUREMENT, AND CONTROL. Manuscript received July 20, 2015; final manuscript received September 12, 2016; published online November 11, 2016. Assoc. Editor: Jingang Yi.

energy affect the validity of the optimization results. In our recent work [12], we refined the optimization scheme by defining a multi-objective cost function that penalizes the sensitivity of performance objective to model parameter uncertainties. This is an offline robust optimization generates open-loop references. It does not include provisions for feedback compensation of uncertainties. In the current paper, we extend our previous work [12] as follows: (1) first we update the UV curing process model in Ref. [13] using our own recent experimental results on UV curing of a composite layer and (2) we then use the experimentally validated process model to pursue robust optimization of a closed-loop scheme that incorporates feedback control at each layer addition.

The main optimization/process performance/objective in layer-by-layer UV curing is minimum overall cure level deviation at the final state. A detailed literature review on how to define the robustness terms for such endpoint optimization of nonlinear systems (including hybrid systems) is given in Ref. [12]. Some of the approaches are minimax approach [14] and multiobjective approach such as sensitivity robustness [15] and mean-variance robustness [16] for regular nonlinear systems, and general game theory such as H_∞ performance index for theoretical hybrid systems [17]. Most of these approaches can be used interchangeably for open-loop and closed-loop robust optimization. For open-loop optimization, the control trajectories are predetermined by adding a robustness term that penalizes the degradation of performance in the presence of parameter uncertainties. An extension of this for closed-loop optimization is repeating the robust open-loop optimization online by incorporating some feedback information of measured or online estimated state variables [18]. However, the feasibility of the robust closed-loop optimization techniques depends on the complexity of the adopted process model and computational burden of the optimization algorithm.

As alternatives for direct robust optimization, conceptually different approaches that include online estimation of uncertain parameters [19] and tracking of the necessary optimality conditions (NOC) [20] can be pursued to accommodate uncertainties. Online estimation suffers from loss of observability for the augmented state and parameter, since often, the distributed state needs to be estimated jointly. The NOC-tracking approach avoids repeated real-time optimization by transforming the optimization problem into a simple feedback control problem. To implement the NOC tracking approach, one can first derive the nominal necessary optimality conditions and then construct neighboring-extremal control around the nominal trajectory that penalizes the variations of NOC due to process parameter uncertainties [20,21]. The feasibility of the NOC-tracking approach has been widely tested for batch and semibatch processes [22]. A similar approach was also applied for a hybrid system of few state variables in Ref. [23]. However, its application for a wider class of problems is limited by the need for full state feedback and the need to solve a two-point boundary-value problem (TPBVP) for the neighboring-extremal control. When applying the NOC-tracking approach for our multimode hybrid dynamic system model of the layer-by-layer UV curing process with growing state dimension, stable solutions of the TPBVP were found hard to obtain due to the instability of backward integration of the costate dynamics, especially when considering a large number of layers.

For the layer-by-layer UV curing process, where the uncertain parameters appear as nonlinear functions of the state, we found that the multi-objective robust performance sensitivity approach is a suitable candidate over other approaches. This is largely because it eliminates the need for a disturbance model of the uncertainty, which is generally difficult to identify or bound accurately for nonlinearly entering parameters. We consider deterministic parameter uncertainties and add a robustness term that penalizes the local sensitivity of the objective function to the parameter uncertainties. The closed-loop robust optimization is then carried in two steps. First, we generate a reference trajectory of the surface temperature (where measurements are possible for feedback control) by optimizing the interlayer hold times for the nominal conditions. Then,

by fixing the interlayer hold times at their nominal optimal values, the UV intensity input at each layering step is determined as a feedback correction that tracks the nominal surface temperature reference while accommodating the uncertainties. The feedback gain vector is selected by optimizing the augmented objective function comprised of the nominal cost function plus the robustness performance sensitivity term. This augmented optimization problem is solved as a minimization problem by augmenting the auxiliary sensitivity dynamics to the process dynamics.

The remainder of the paper is organized as follows: Section 2 gives a generalized 1D model for a UV curing process, and discusses a set of experiments and model validation for a composite laminate that constitutes glass fiber and unsaturated polyester resin. Section 3 discusses the closed-loop robust optimization control implementation including the hybrid modeling formulation of the layer-by-layer build-up process. Section 4 offers demonstrative numerical simulation results and discussions. Section 5 gives the conclusions of the work.

2 Ultraviolet Curing Process Model and Experimental

2.1 One-Dimensional UV Curing Process Model. Consider the 1D UV curing process setup for a fiberglass composite laminate shown in Fig. 1. The process model has three submodels: (1) cure kinetics model that predicts the cure level evolution; (2) heat transfer model that accounts for heat generation due to exothermic reactions; and (3) a UV radiation attenuation model that accounts for the attenuation of UV intensity across the layer in the z -direction according to Beer-Lambert's law [24]. Other modeling considerations can be referred from Refs. [13] and [25]. The following coupled partial differential equation (PDE)–ordinary differential equation (ODE) system, along with the boundary and initial conditions, summarize 1D process model for UV curing of a single layer:

$$\rho c_p \frac{\partial T(z, t)}{\partial t} = \frac{\partial}{\partial z} \left(k_z \frac{\partial T(z, t)}{\partial z} \right) + v_r \Delta H_r \rho_r \frac{d\alpha(z, t)}{dt} \quad (1a)$$

$$-k_z \frac{\partial T(0, t)}{\partial z} + \vartheta I_0 = h(T(0, t) - T_\infty) \quad (1b)$$

$$\frac{\partial T(l, t)}{\partial z} = 0 \quad (1c)$$

$$T(z, 0) = T_0(z) \quad (1d)$$

$$\frac{d\alpha(z, t)}{dt} = s_0^g \exp(-\lambda p z) I_0^g K_D(\alpha) [K_1(T) + K_2(T)\alpha(z, t)] (1 - \alpha(z, t))(\bar{B} - \alpha(z, t)) \quad (1e)$$

$$K_D(\alpha) = \frac{1}{1 + \exp(\xi(\alpha(z, t) - \alpha_c))} \quad (1f)$$

$$K_1(T) = A_1 \exp\left(\frac{-E_1}{RT_{\text{abs}}(z, t)}\right) \quad (1g)$$

$$K_2(T) = A_2 \exp\left(\frac{-E_2}{RT_{\text{abs}}(z, t)}\right) \quad (1h)$$

$$\alpha(z, 0) = \alpha_0(z) \quad (1i)$$

$$\lambda_c = b_r + b_{pI} s_0 \quad (1j)$$

where ρ and c_p are the (homogenized) density and specific heat capacity of the composite laminate, respectively; k_z is the thermal conductivity of the laminate in the z -direction; $T(z, t)$ is temperature distribution at depth z and time t ; v_r is volumetric fraction of

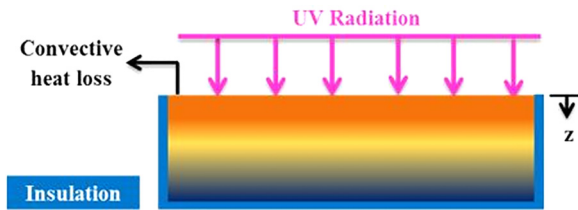


Fig. 1 Schematic for a UV curing process model

resin in the composite matrix; ρ_r is density of resin; and ΔH_r is polymerization enthalpy of resin conversion; ϑ is absorptivity constant of the UV radiation at the boundary; I_0 is UV input intensity at the surface; h is convective heat transfer at the top boundary; l is the thickness of a single layer; T_∞ is constant ambient temperature; $d\alpha(z,t)/dt$ is the rate of cure conversion (rate of polymerization); s_0 is photoinitiator concentration; p & q are constant exponents; b_r is absorption coefficient in the resin plus fiber without photoinitiator; b_{p1} is absorption coefficient due to photoinitiator; λ_c is the absorption coefficient in the resin plus fiber; \bar{B} is constant parameter related to reaction orders; ζ is diffusion constant; α_c is critical value of cure level; A_1 & A_2 are pre-exponential rate constants; E_1 & E_2 are activation energies; R is gas constant; $T_{\text{abs}}(z,t)$ is absolute temperature in Kelvin; and $\alpha(z,t)$ is cure level/state distribution.

2.2 Experimental Model Verification. In our previous work [13], we identified some of the above process parameters from partial experiments that include in-process UV transmission and thermal measurements. Measurement of the UV transmission through the composite laminate with and without photo-initiator is used to determine the UV attenuation constant λ . Model parameters related with heat convection and conduction were identified and validated based on a separate set of temperature measurements recorded after complete cure of the composite laminate which excludes the heat generation term (cure kinetics model) from the heat transfer model. The rest of the parameters related to cure kinetics (A_1 , A_2 , E_1 , E_2 , and \bar{B}) were extracted from the literature [26], which considered the UV curing of unsaturated polyester resins without fibers. Then, we modified the parameters from Ref. [26] based on the temperature measurements recorded while curing composite laminate samples. However, cure kinetics experiments were not conducted for the selected resin system.

For the present paper, we conducted explicit cure kinetics studies for unsaturated polyester resin using Q2000 differential scanning calorimeter (DSC) with a photocalorimetry accessory (PCA) from TA instruments. The PCA contains UV light guide and UV power supply of an Omni-cure s2000 powered by high-pressure mercury lamp. It emits light in the range of 320–500 nm, with peak emission at 365 nm. The UV light guide is used to guide the UV radiation from the power source to affect only the sample and reference pan placed inside the chamber of the DSC device.

The rate of the photopolymerization reactions in UV curing is affected by the concentration of the photoinitiator, curing temperature, intensity, and exposure time of the target to the UV radiation [26]. To evaluate and model the influence of these process parameters, three sets of isothermal kinetics studies were conducted using photo-DSC. The photo-DSC instrument is used to measure heat flow rate per sample weight when curing photo-initiated unsaturated polyester resin sample. The heat flow was recorded for three sets of experiments intended to investigate the effect of photoinitiator concentration (Experiment #1), curing temperature (Experiment #2), and UV intensity (Experiment #3). These experiments were conducted by varying one parameter at time while keeping the rest constant as summarized in Table 1.

For each experiment run, photocuring is initiated first by placing the photo-initiated resin and reference sample inside the DSC sample chamber using the Aluminum pan. Then, a desired UV intensity was applied to the resin sample and reference pan by adjusting the light guide adapter base position from the sample by using the positioning screw in addition to appropriate filter installed in the light guide head. Finally, the resin sample was set to the desired curing temperature for 1 min before the curing is initiated to maintain an isothermal curing condition. Then, the UV power was turned on to initiate the UV curing and the exothermic heat released due to photopolymerization was measured. The results are plotted in Figs. 2–4 for the three experiment sets.

The experimental results plotted in Figs. 2–4 show the evolution of the heat of polymerization in terms of exothermic heat generation per sample weight (W/g). As shown in the plots, the highest rate of cure (or faster polymerization) is associated with highest photoinitiator concentration, temperature, and UV intensity. Some other observations from the results in Figs. 2–4, including the peak time corresponding to maximum heat flow and total heat of reaction, are summarized in Table 1. The total heat of polymerization ΔH_p is calculated by integrating the net heat flow curve defining the base line heat flow $\dot{q}_b(t)$ for the total length of cure duration. Then, the progress of cure conversion α from the experimental data is calculated by normalizing the integrated net heat flow at time t to the total heat of polymerization while the cure rate $d\alpha/dt$ is calculated by normalizing the net heat flow at time t to the total heat of polymerization. The mathematical relationship of the polymerization heat flow rate to the cure rate and cure conversion is summarized below:

$$\Delta H_p = \int_0^{t_f} (\dot{q}(t) - \dot{q}_b(t)) dt \quad (2a)$$

$$\alpha(t) = \int_0^{t_f} \frac{(\dot{q}(t) - \dot{q}_b(t)) dt}{\Delta H_p} \quad (2b)$$

$$\frac{d\alpha(t)}{dt} = \frac{(\dot{q}(t) - \dot{q}_b(t))}{\Delta H_p} \quad (2c)$$

Note that from the Table 1, the largest total heat of polymerization is close to the one published in Ref. [27] for the same resin system of the unsaturated polyester. Here, we use a ΔH_p value of 315 J/g in the following analysis to compare the cure conversion for different curing conditions.

2.3 Prediction of Cure Kinetics Parameters. In principle, the photopolymerization process is characterized by three main reactions: photo-initiation, propagation, and termination, which can be captured via complex mechanistic models [28]. In the current paper, we develop one phenomenological model of the cure kinetics for the whole curing process where the related parameter constants were identified based on the cure kinetics experiment discussed above. This model can be made to capture the dominant effects in the curing kinetics by introducing parameters that account for different aspects of the photochemical reaction. In the literature, different forms of autocatalytic models are used to predict the in-process cure rate of UV-curable resin systems [29,30]. In most proposed models, the effect of all three fundamental process parameters: photoinitiator, temperature, and UV intensity are not modeled explicitly except in Ref. [27], which offered the following model:

$$\frac{d\alpha}{dt} = s_0^q I_0^p g(T, \alpha) \quad (3a)$$

$$g(T, \alpha) = K(T) \alpha^m (1 - \alpha)^n \quad (3b)$$

Table 1 Summary of cure kinetic studies of photo-initiated resin of unsaturated polyester via photo-DSC

Experiment #	Cure temperature (°C)	UV intensity (mW/cm ²)	Photoinitiator concentration (wt.%)	Total heat of reaction (J/g)	Peak time (min)
1	25	50	0.05	274	1.28
			0.1	287	1.11
			0.25	294	0.71
			0.5	303	0.56
			0.1	307	0.46
			2	315	0.38
2	25	50	0.1	287	1.11
				298	0.69
				302	0.56
3	25	30	0.1	270	1.46
		50	0.1	287	1.11
		70	0.1	293	0.75

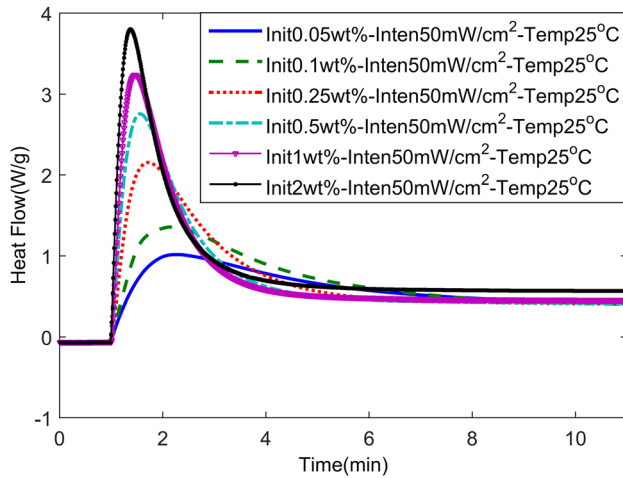


Fig. 2 Measured isothermal heat flow for varying photoinitiator

where m & n are reaction orders and are assumed to satisfy, $m + n = 2$. The rest of the parameters in Eq. (3) are as defined with Eq. (1) above. However, in the current paper, we make changes to Eq. (3b) to make the model more suitable for our control and optimization computations. This change, already included in the model summarized in Eq. (1), is to use the form

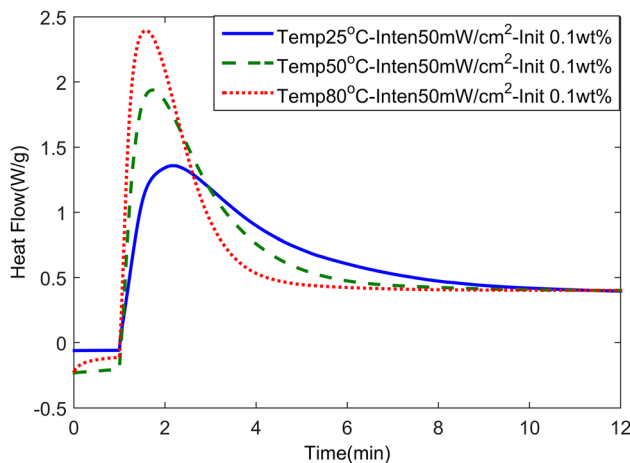


Fig. 3 Measured isothermal heat flow for varying curing temperature

$$g(T, \alpha) = [K_1(T) + K_2(T)\alpha](1 - \alpha)(\bar{B} - \alpha) \quad (4)$$

In Eq. (3), the reaction order m is determined by taking derivative of $d\alpha/dt$ with respect to α and setting it to zero. This results in $m = 2\alpha_p$, where α_p is the cure conversion at maximum cure rate. The exponent terms p & q are determined based on the experimental data recorded at room temperature by varying photoinitiator concentration and UV intensity, respectively. Then, the activation energy E appearing in the Arrhenius term $K(T) = A \exp(-E/RT_{abs})$ is determined based on the experimental data measured by varying curing temperatures. For the detail derivation and identification of model parameters, one can also refer to Ref. [26]. For the modified model with Eq. (4), we use the exponent terms p & q identified from the previous model to determine the Arrhenius components K_1 & K_2 and reaction constant \bar{B} . These constant terms are determined by fitting the experimental data of cure rate $d\alpha/dt$ to the cure conversion α using the nonlinear Levenberg–Marquardt algorithm for curve fitting [31]. Then, parameters related to Arrhenius components of K_1 & K_2 such as activation energies E_1 & E_2 and the pre-exponential rate constants A_1 & A_2 are determined by developing linear curve fits to the K_1 & K_2 versus $1/T$ data for varying curing temperature.

The rate of cure from the experimental data and those predicted by the two versions of phenomenological model are compared in Fig. 5. In Fig. 5, model-1 represents the modified kinetics model given with Eq. (4) (which we find computationally expedient for the optimizations to be outlined later), while model-2 represents the one given by Eq. (3). The initial and peak rates of cure are best captured by model-2 while some tolerable deviation is observed for the prediction by model-1. However, for higher cure temperatures ($T = 80^\circ\text{C}$), the prediction by model-2 has larger

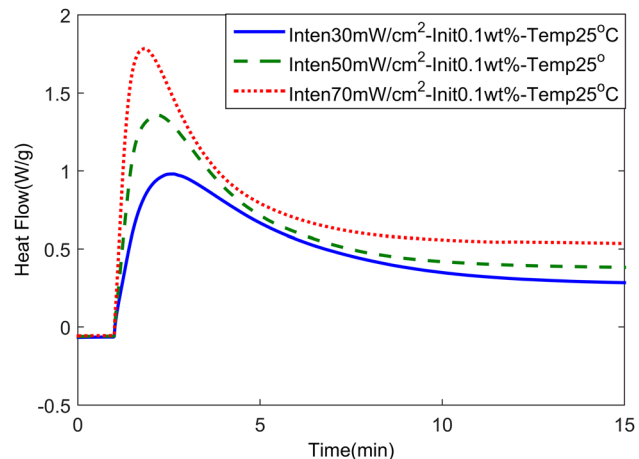


Fig. 4 Measured isothermal heat flow for varying UV intensity

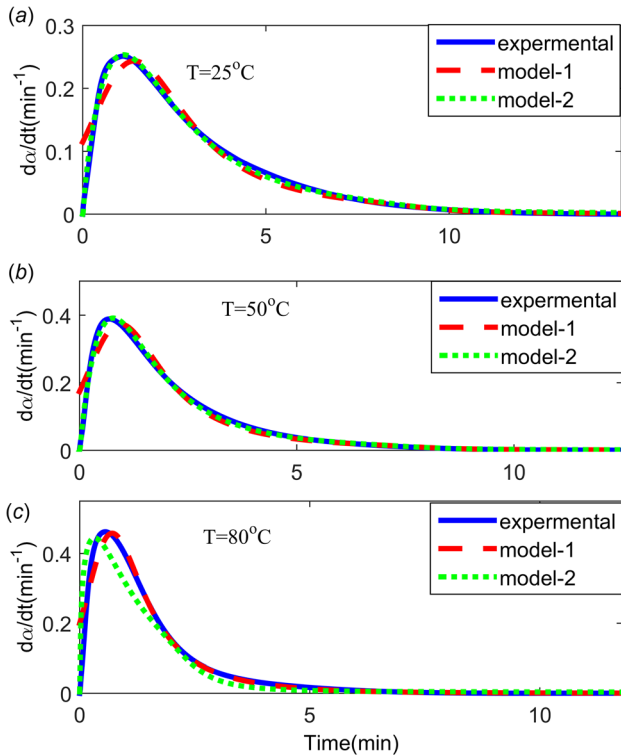


Fig. 5 Comparison of measured and predicted cure rate for varying curing temperature: (a) $T = 25^\circ\text{C}$, (b) $T = 50^\circ\text{C}$, and (c) $T = 80^\circ\text{C}$

overall error than model-1. This can be explained by the relationship of the Arrhenius term K versus $1/T$. For the prediction by model-2, this relationship is not linear for the entire range of curing temperature where constant activation energy is calculated. Similar observation was also made in Ref. [26], which suggested change of the activation energy for curing temperatures above 60°C for a similar resin system. For the prediction by model-1, a linear relation is obtained with constant activation energy for the entire curing temperature.

The complete set of experimentally identified UV curing process parameters including the attenuation constant, convective heat transfer coefficients, and other thermal properties of the

Table 2 Parameter values used in the simulations

Symbol	Parameter	Value
ρ	Density of composite	1.69 g/cm ³
c_p	Specific heat of composite	1.14 J/g °C
k_z	Thermal conductivity of composite	0.0026 W/cm °C
ρ_r	Density of resin	1.1 g/cm ³
h	Convective heat transfer	0.0036 W/cm ² °C
ΔH_r	Polymerization enthalpy of resin	315 J/g
E_1 & E_2	Activation energies	[2.87 & 3.87] KJ/mol
A_1 & A_2	Pre-exponential factors	[0.02 & 2.63] min ⁻¹
R	Gas constant	8.314 J/mol K
s_0	Photoinitiator concentration	0.1 wt.%
λ	UV attenuation constant	7 cm ⁻¹
T_∞	Ambient temperature	25 °C
B	Cure kinetics constant	1.22
v_r	Volume fraction of resin	0.6
p & q	Constants exponents	0.53 & 0.54
ϑ	Absorptivity of UV radiation	0.85
α_c	Critical cure level	0.92
ξ	Diffusion constant	159.4

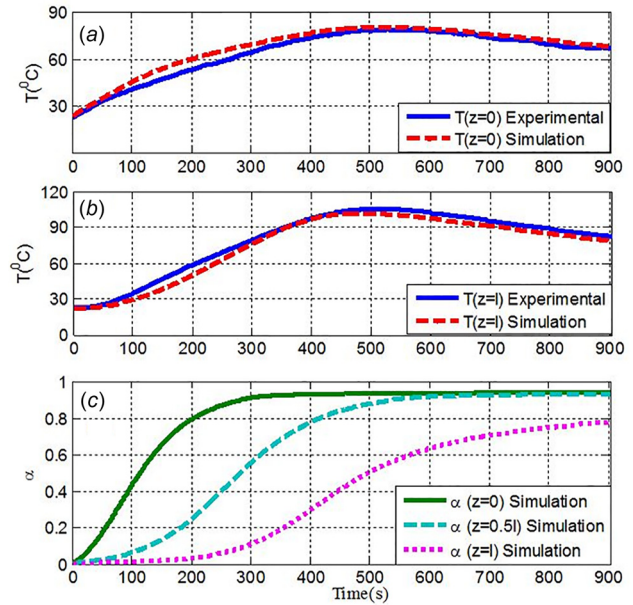


Fig. 6 Comparison of simulated and measured temperature: (a) top surface temperature, (b) bottom surface temperature, and (c) simulated cure conversion

composite are summarized in Table 2 for the modified kinetic model (model-1). To validate the modified process parameters, we simulated the UV curing process model in (1a)–(1i) and compared the results measurements conducted while curing a sample of 5 mm thickness with applied UV intensity of 100 mW/cm². The simulated and measured in situ cure temperatures in the composite laminate (top ($z = 0$) and bottom ($z = l$) surface) are shown in Figs. 6(a) and 6(b). The simulated cure state evolution at the top, middle, and bottom of the sample are also plotted in Fig. 6(c). The in situ temperature measurement (via thermocouples), cure sample preparation, and simulation considerations are detailed in Ref. [13] and are skipped here for brevity.

In Fig. 6, the process parameters identified through three different experimental studies: kinetics study, UV transmission measurement, and in situ temperature measurement result in a good match of simulated temperature with that of the measured one. The corresponding cure conversion simulation in Fig. 6(c) predicts a complete cure for layers at the top and maximum of over 80% conversion for the bottom. Although there was no direct measurement available to quantify the local cure conversion, for the cured sample, an average hardness value of about 98% of the top surface is measured at the bottom surface. This relative hardness value can be used to infer that the bottom cure conversion is closer to the top one.

The identified process parameters given in Table 2 will be used for simulation studies on the model-based robust optimal control schemes proposed and detailed in the rest of the paper.

3 Closed-Loop Robust Optimal Control Via Hybrid System Modeling

3.1 Overall Control Scheme. The need for optimal control of the UV curing process can be motivated by examining the simulated cure state shown in Fig. 6(c) above. For the 5 mm sample thickness, the top surface comes to complete cure in faster time and continues to over-cure while the bottom cures slowly with attenuated UV intensity reaching there. For larger sample thicknesses, this deviation will be higher and there may be even no cure conversion at the bottom because of attenuation. A layer-by-layer curing process can be systematically optimized to overcome this attenuation challenge for thick composite laminate

fabrication. We propose to use the above process model in the optimizations and incorporate feedback means for accommodating process uncertainties.

The proposed robust optimization and closed-loop control scheme is depicted schematically in Fig. 7. The high level or outer-loop control solves an offline optimization of the layer-by-layer curing process using the hybrid modeling framework to be described below. This optimization considers nominal process model parameters and it provides: (1) a reference trajectory of the surface temperature, T_{iref} and (2) the nominally optimal inter-layer hold times τ_i . In this paper, the nominal UV intensity, u_{inom} is taken as constant control input for all stages of the layer addition while the layering times are selected optimally. Both u_{inom} and τ_i form the augmented feed forward control inputs to the process.

The reference surface temperature trajectory is to be tracked by the low-level (inner-loop) feedback controller. The feedback law is constructed as an output feedback controller of the form

$$u_i = u_{inom} + L_i(T_{isurface} - T_{iref}) \quad (5)$$

where $T_{isurface}$ is the measured boundary temperature and L_i is stagewise static feedback gain at each layer addition. The feedback control signal is computed to track the bottom boundary temperature instead of the top (open) boundary. For the top boundary, there is a sudden drop of temperature as new layers add on (inter-layer cooling) and this may result in undesirable spikes in the feedback control signal. For the bottom boundary, this sudden drop at the interface does not show up immediately because of the poor thermal conductivity of polymer materials.

The feedback term considered in Eq. (5) is intended to compensate for degradation of the nominal optimality due to process uncertainties. The static feedback gains themselves are then selected by a separate offline optimization that considers the parameter uncertainties. An explicit optimization scheme is

discussed below after elaborating on the formulation of the layer-by-layer UV curing process as a hybrid system.

3.2 Formulation of the Layer-By-Layer UV Curing Process as a Hybrid System. During the layer-by-layer build-up process, the successive addition of a new layer changes the dynamics of the processes. This change introduces new initial and boundary conditions as well as a growing spatial domain that results in different process dynamics after each layer addition. The layer addition process can be treated as a switching of the dynamics from one mode to another with predefined switching sequence. This mode switch represents a discrete event on the otherwise continuous curing process with its associated thermal evolution and cure-reaction phenomena. This makes the layer-by-layer curing process a naturally switched hybrid system. This hybrid system view of the layer-by-layer curing process is depicted schematically in Fig. 7. In the following, a “mode” represents the state dynamics (PDE–ODE pair given by Eq. (1)) before or after the addition of a new layer. The first mode (Mode 1) has only one layer, and all other modes have more, in increasing numbers, as shown in the top block of Fig. 7. The mode switching times are denoted by τ_1 through τ_N . In this hybrid system view, the switching/layering times and the UV radiation input can both be considered as control variables that can be manipulated for a desired effect, in this case, for minimization of cure level deviations in a multilayer part. Further details of this hybrid system realization of the layer-by-layer curing process, including additional assumptions and observations useful for extending the 1D UV curing process dynamics to the layer-by-layer manufacturing processes, are given in our previous paper [11,32]. Here, we summarize the mathematical description of the layer-by-layer process in the hybrid framework.

Denoting the thickness of the part after the i th layer is added by il and introducing a coordinate transformation $y = il - z$ between

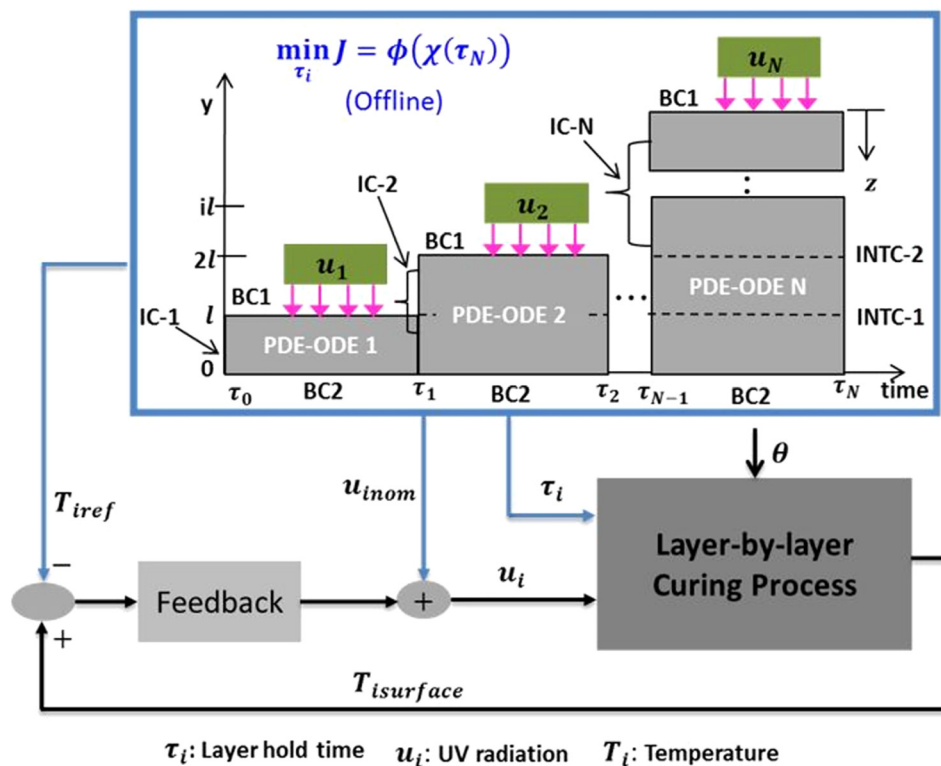


Fig. 7 A hybrid system formulation of the layer-by-layer curing process with closed-loop control

the global y -axis and the local z -axis, and introducing notations $T_i^i(y, t)$, $T_y^i(y, t)$, $T_{yy}^i(y, t)$ and $\alpha_i^i(y, t)$ for $\partial T^i(y, t)/\partial t$, $\partial T^i(y, t)/\partial y$, $\partial^2 T^i(y, t)/\partial y^2$ and $\partial \alpha^i(y, t)/\partial t$, respectively, the state evolution for mode i in the time interval, $t \in [\tau_{i-1}, \tau_i]$ takes the form

$$T_i^i(y, t) = aT_{yy}^i(y, t) + b(y)f^i(T^i(y, t), \alpha^i(y, t), L_i, \theta) \quad \text{on } \Omega_\tau^i \quad (6a)$$

$$T_y^i(il, t) + eI_0 = c(T^i(il, t) - T_\infty) \quad \text{on } \Gamma_1^i \quad (6b)$$

$$T_y^i(0, t) = 0 \quad \text{on } \Gamma_2^i \quad (6c)$$

$$\alpha_i^i(y, t) = d(y)f^i(T^i(y, t), \alpha^i(y, t), \theta) \quad \text{on } \Omega_\tau^i \quad (6d)$$

$$f^i(T^i(y, t), \alpha^i(y, t), L_i, \theta) = (u_{inom} + L_i(T_{isurface} - T_{iref}))^p K_D^i(\alpha) \{K_1^i(T) + K_2^i(T)\alpha^i(y, t)\}(1 - \alpha^i(y, t)) (\bar{B} - \alpha^i(y, t)) \quad \text{on } \Omega_\tau^i \quad (6e)$$

where both the temperature state $T^i(y, t)$ and cure state $\alpha^i(y, t)$ evolve in the spatiotemporal domain defined by $\Omega_\tau^i = [0, il] \times [\tau_{i-1}, \tau_i]$, $0 \leq \tau_0 < \tau_1 < \dots < \tau_N < \infty$. The boundary conditions are also defined on $\Gamma_1^i = \{il\} \times [\tau_{i-1}, \tau_i]$ and $\Gamma_2^i = \{0\} \times [\tau_{i-1}, \tau_i]$. $\theta \in \mathcal{R}^m$ is a vector of uncertain parameters; and $d(y) = s_0^q \exp(-\lambda p(il - y))$, $b(y) = d(y)(v_r \Delta H_r \rho_r / \rho c_p)$, $a = k_z / \rho c_p$, $c = h/k_z$, and $e = \vartheta/k_z$; K_D , K_1 , and K_2 are as given in (1f)–(1h). In the following analysis, for brevity, we use $f^i(T^i, \alpha^i, L_i, \theta)$ instead of $f^i(T^i(y, t), \alpha^i(y, t), L_i, \theta)$, dropping the spatial and temporal indices of the state. Note that in Eq. (6), the UV radiation I_0 is the UV input $u_i(t)$. For the UV curing process, the main uncertain parameters may include cure kinetics parameter constants: $\theta = [E_1, E_2, \bar{B}]'$. To avoid confusion with the temperature state T , the transpose of a vector is denoted by $[\cdot]'$ instead of the usual $[\cdot]^T$.

For two or more layers, at the interface of new and earlier layers, the interface conditions (INTC) at $i = 1, 2, \dots, N - 1$ are defined as

$$[k_z T_y^i(il, t)]_{\text{new layer}} = [k_z T_y^i(il, t)]_{\text{previous layer}} \quad (7a)$$

$$[T^i(il, t)]_{\text{new layer}} = [T^i(il, t)]_{\text{previous layer}} \quad (7b)$$

At each switching time τ_i , $i = 1, 2, \dots, N - 1$, the transition to the new mode defines new initial conditions for the next mode. This is described compactly for both the temperature and cure state by

$$T^{i+1}(y, \tau_i^+) = F^i(T^i(y, \tau_i^-), T_0(y)) \quad (8a)$$

$$\alpha^{i+1}(y, \tau_i^+) = G^i(\alpha^i(y, \tau_i^-), \alpha_0(y)) \quad (8b)$$

where $T^i(y, \tau_i^-)$ and $T^{i+1}(y, \tau_i^+)$ are the left-hand and right-hand limit values of the temperature state in mode i and mode $i + 1$, respectively, at the switching time τ_i . $F^i : \Omega^i \rightarrow \Omega^{i+1}$ is the mode transition operator for the temperature state at switching time τ_i defined over $\Omega^i \in [0, il]$. Since both states coexist in the spatial domain in all modes, similar definitions hold for the cure state (8b) as well.

To give a particular example of the mode transition operator for this application, the starting temperature at switching time τ_i is taken as the average temperature at the interface of the new layer and the layer in the curing process. The cure state at the interface is taken as that of the cure state already in the curing process because cure conversion is an irreversible process. For all other

locations in the domain away from the interface (all previous layers already being cured), the initial values of the temperature and cure states in the new mode take their values from the end of the previous mode. The initial value of all state elements corresponding to locations in the new layer will take on ambient conditions.

Temperature state mode transition operator

$$F^i(T^i(y, \tau_i^-), T_0(y)) = \begin{cases} T^i(y, \tau_i^-), & 0 \leq y < il \\ \frac{1}{2}(T^i(y, \tau_i^-) + T_0(y)), & y = il \\ T_0(y), & il < y \leq (i + 1)l \end{cases} \quad (9a)$$

Cure state mode transition operator

$$G^i(\alpha^i(y, \tau_i^-), \alpha_0(y)) = \begin{cases} \alpha^i(y, \tau_i^-), & 0 \leq y \leq il \\ \alpha_0(y), & il < y \leq (i + 1)l \end{cases} \quad (10a)$$

Equations (6)–(10) complete the hybrid formulation for the layer-by-layer UV curing process.

3.3 Closed-Loop Robust Optimization. While the above hybrid formulation admits both the UV input and the layering times as optimizable control inputs, in the current work, after some analysis, we chose to separate the utility of these control inputs as follows. The layering times will be selected via offline optimization using the nominal hybrid process model. The UV input is to be manipulated online around a nominal (feed forward) setting to accommodate process uncertainties via optimal feedback (see Eq. (5)).

Given the above, for the hybrid system described by Eqs. (6)–(10), the optimal control problem can be posed as one of finding the optimal switching time vector $[\tau_1, \dots, \tau_N]'$ and the layer-by-layer static feedback gain vector $[L_1, \dots, L_N]'$ that minimizes a cost function of the following form:

$$J(\tau_i, L_i, \theta) = (1 - \beta) \int_{\Omega^N} \bar{g}(\chi^N(y, \tau_N^-), \bar{\theta}) dy + \beta \sum_{j=1}^m \left\{ \left[\int_{\Omega^N} \frac{\partial \bar{g}(\chi^N(y, \tau_N^-), \bar{\theta})}{\partial \chi^N} * S^{\chi^N, j}(y, \tau_N^-) dy \right]^2 + \int_{\Omega^N} [S^{\chi^N, j}(y, \tau_N^-)]^2 dy \right\} \quad (11)$$

where \bar{g} represents the desired objective function at final time τ_N . The second term in Eq. (11) defines the robustness consideration with sensitivity of the nominal cost function to parameter changes; $S^{\chi^N, j}(y, \tau_N^-) = \partial \chi^N(y, \tau_N^-) / \partial \theta_j$ is the sensitivity of final state w.r.t parameter uncertainty; and $\chi = [T, \alpha]'$ is augmented state of temperature and cure level. The initial time τ_0 and state $\chi(y, \tau_0)$ are assumed fixed, while the final time τ_N and state $\chi(y, \tau_N^-)$ are free to be optimized. θ is again the vector of uncertain parameters. For normalized state variables, the weighting function β ($0 \leq \beta \leq 1$) is considered as a robustness measure that defines a tradeoff between good nominal performance and minimizing performance loss due to uncertainty. The choice of β reflects the emphasis given by the designer to accommodate expected uncertainty. The higher the value of β , the more weight is given to the sensitivity of the cost (final state) to the expected uncertainty, which leads to final state optimal inputs that are less sensitive to this uncertainty. However, this comes at a loss of nominal performance. Alternatively, if there is a high confidence in model parameters, then the designer can select a small value

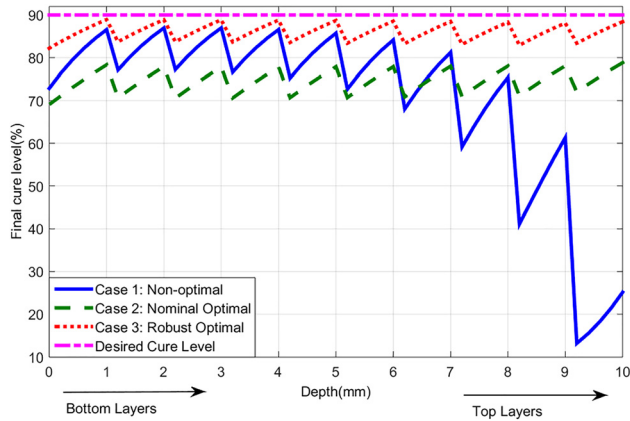


Fig. 8 Final cure level profile with +10 % parameter deviation in E_2 and -10 % parameter deviation in B

of β . Some simulation results are included later to illustrate this tradeoff.

In Eq. (11), in addition to the first moment sensitivity of the nominal cost function; we included additional quadratic final state sensitivity term to improve the performance of the robust optimization. The first moment consideration alone prematurely stops the optimization iteration as the actual cure state deviation approaches to zero before the cure state sensitivity goes to zero. The addition of the quadratic sensitivity term helped to overcome this challenge.

The robust optimization problem (11) subjected to process dynamics constraints (6)–(10) is solved in two steps. First, the layer addition time vector is optimized by fixing θ at its nominal value $\bar{\theta}$ and setting $\beta = 0$. This gives nominal layering times and the open-loop nominal optimal trajectory for the temperature state. Then, fixing the layering times at their nominal optimal values, the static feedback gain vector is optimized to track the nominal reference trajectory of the bottom surface temperature to accommodate uncertainty modeled by selecting the robustness weight $\beta > 0$. For detailed derivations of the optimality conditions and numerical optimization algorithm for the case of the nominal optimization problem (with only the first term in the objective, $\beta = 0$), the reader is referred to our previous work [11].

For $\beta > 0$ with uncertainty considerations, conventional optimization techniques cannot be used directly because the added sensitivity terms for robustness analysis contain sensitivity states (e.g., $\partial \chi^N(y, \tau_N^-) / \partial \theta$), which are not explicit in the process dynamics. As a result, derivation of additional auxiliary dynamics

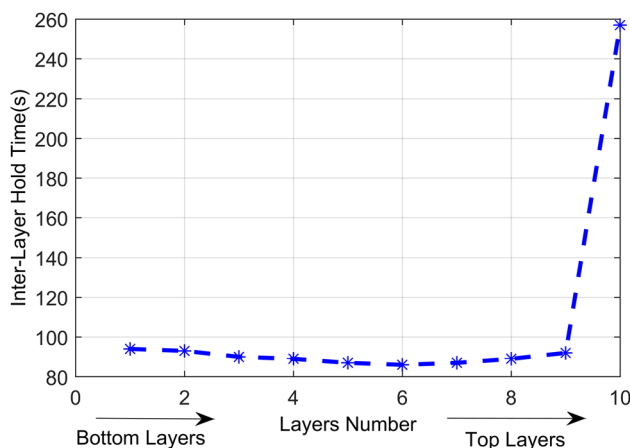


Fig. 9 Optimized interlayer hold times for nominal optimization case (Case 2)

is required to solve for the sensitivity state directly. Then, the robust optimization problem (11) can be solved as a regular minimization problem by augmenting the auxiliary sensitivity dynamics to the process dynamics. In the current paper, for a solution of robust optimal static feedback gain, the optimality conditions along with the sensitivity dynamics constraints can be derived following the derivation procedure detailed in Ref. [12].

4 Results and Discussions

In this section, we present simulation results to demonstrate the feasibility of the proposed closed-loop robust optimization scheme by simulating composite laminate fabrication via the layer-by-layer UV curing process. The composite laminate constitutes fiberglass and unsaturated polyester resin. Here, we are interested in achieving a through cure in all layers with minimum overall deviation at the end of the curing process by optimizing the interlayer hold times and manipulating the UV radiation input via the feedback of surface temperature. The desired optimization objective is described by selecting a nominal terminal cost function g in Eq. (11) of the form

$$\bar{g}(\chi^N(y, \tau_N^-, \bar{\theta})) = 0.5\{\alpha^N(y, \tau_N^-) - \alpha_d(y)\}^2, \quad y \in [0, Nl] \quad (12)$$

For the simulation study, the thermal properties of unsaturated polyester resin are extracted from published work [33]. For the fiberglass, E-glass thermal properties such as thermal conductivity ($k_z = 0.01 \text{ W/cm}^\circ\text{C}$), specific heat ($c_p = 0.8 \text{ J/g}^\circ\text{C}$), and density ($\rho = 2.54 \text{ g/cm}^3$) are used. The resin volume fraction is assumed to be 60% for computing the average thermal properties of the composite laminate. Other experimentally verified nominal process parameters are summarized in Table 2 given in Sec. 2.2.

For the process simulation and implementation of the optimization algorithm, a 10-node spatial discretization is adopted to convert the temperature and associated state PDEs to a set of ODEs in time, for each layer. In the simulations, we considered a layer made from three fiber plies with an approximate thickness of 1 mm per layer. The results are generated for a sample thickness of 10 mm with total number of ten layers. A cure level of 90% was set as a desired final cure level. A constant UV-intensity of 100 mW/cm^2 is used for the entire curing duration as the nominal feedforward UV input, while the layering times (the other feed forward control) are determined by the nominal optimization.

We illustrate the advantages of the proposed closed-loop robust optimization scheme by comparing the results of the following cases. Case 1: A nonoptimal approach with equal-interval layering time and constant UV input; Case 2: Nominal optimal approach with nominal optimal layering time control and constant UV

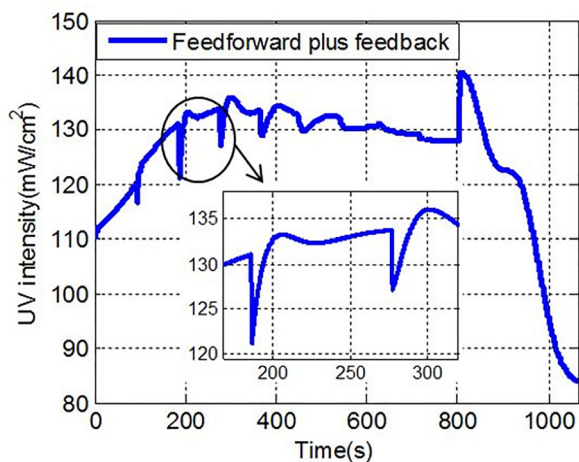


Fig. 10 Control input of UV intensity for robust optimization case (Case 3)

Table 3 Optimized values of layering times and feedback gains

Optimized variable	Layer #									
	1	2	3	4	5	6	7	8	9	10
Interlayer hold times	94	93	90	89	87	86	87	89	92	257
Feedback gains	-59	-54	-52	-44	-37	-35	-34	-32	-29	-46

input; and Case 3: Closed-loop robust optimization approach with nominal optimal layering time control and constant feedforward plus optimized gain-feedback UV input control (Eq. (5)).

For the nonoptimal approach of equal-interval layering time (Case 1), the length of overall curing time is kept the same as that of the overall curing duration of the nominal optimal approach (Case 2). For the nominal optimal case, the optimization is executed until the desired performance is achieved. For the closed-loop robust optimal approach (Case 3), the optimization is executed until the robustness term of the cost function defined by system sensitivity reaches near zero. The overall execution time for optimization case 2 took about 13.24 min while execution time for case 3 took a relatively longer time about 34.56 mins because of added dynamics constraint related to sensitivity. The comparison of the results in final cure state distribution in the three cases, along with corresponding control inputs, is given in Figs. 8–10 below.

For the robust optimization cases, first we investigated the effect of each uncertain parameter in the vector $\theta = [E_1, E_2, \bar{B}]^T$ on the nominally optimal result considering $\pm 10\%$ deviation for each parameter, taken one at a time. The effect of positive and negative sides of the parameter deviations is not symmetric. This can be explained by the differences in cure rate with increase and decrease of these parameters. For example, in case of parameter E_2 , the deviation in the positive direction decreases the cure rate and this results in incomplete cure and it leads to larger deviations of the final cure level as the parameter deviates more. Whereas the deviation in the negative direction increases the cure rate but the rate of increment after a critical cure level of $\alpha_c = 0.92$ (which is closer to the desired cure level of $\alpha = 0.9$) is not significant because of the diffusion-controlled effect. With the current set of experimentally validated process parameters, we also found that a decrease of \bar{B} is as equally important as an increase of E_2 . In the simulation results plotted below, we presented the results where the cited worst-case uncertainty in E_2 & \bar{B} is added to the process/plant model and the robust optimizations are done with the weight $\beta = 0.25$.

Figure 8 shows that for the nonoptimal case (Case 1) of equal-interval layering time, a slight over cure is observed for the bottom layers while unacceptable cure level is achieved in the last few top layers compared to the desired cure level. The other two optimized results (Cases 2 and 3) offer a much better uniformity in the final cure level distribution as compared to the nonoptimal case. However, the nominal optimization result suffers from process uncertainties. The worst-case consideration of $a + 10\%$

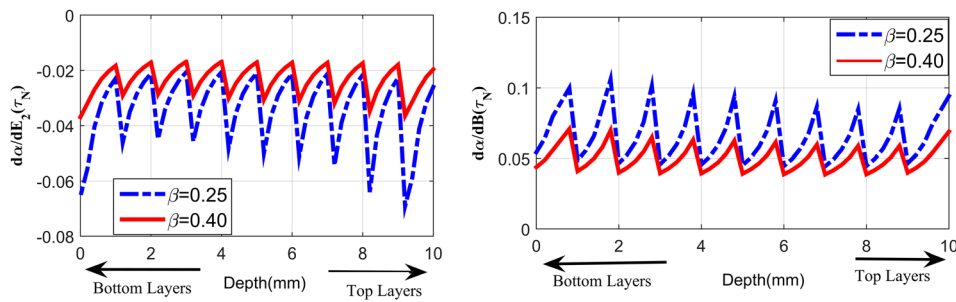


Fig. 11 Sensitivity of the final cure state ($d\alpha/d\theta$ is normalized with respect to its maximum)

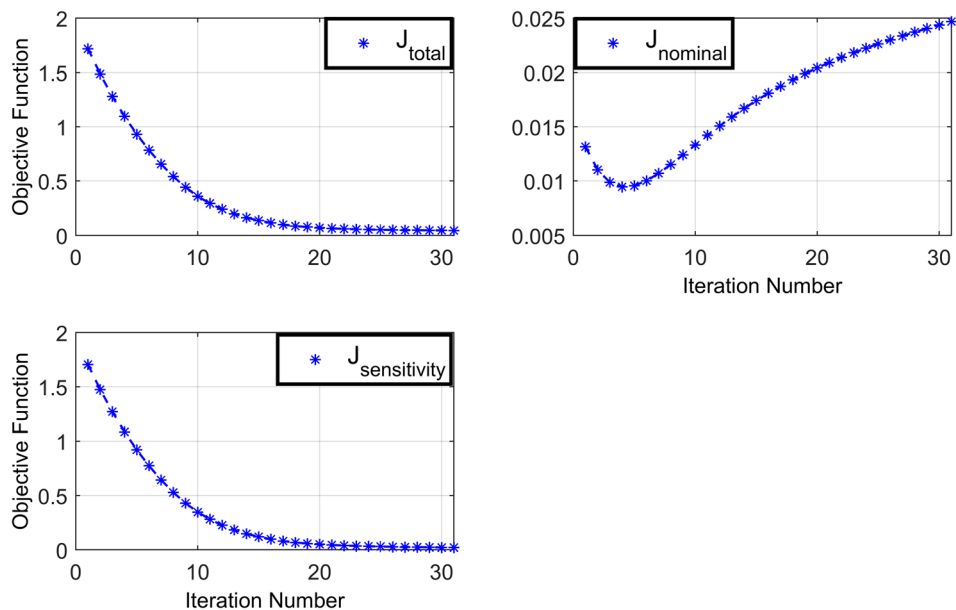


Fig. 12 Convergence of computational algorithm (with $\beta = 0.25$)

deviation in E_2 and a -10% deviation in \bar{B} in the process model reduces the nominal result of near through cure (about 90%) to about 75% on average. This cure level deviation of more than 15% is significantly reduced by the proposed robust optimization of the layer-by-layer feedback gains (Case 3).

Figure 9 shows the trend of the nominal optimal interlayer hold times. It first decreases from its value for the first few bottom most layers, seems to settle to a minimum for the middle layers before becoming highest in magnitude at the end as one adds layers from the bottom to top. The numerical values of this interlayer hold times are summarized in Table 3 along with layerwise feedback gains. The longer hold times computed at the bottom most layers can be explained by a need to precompensate the anticipated large UV attenuation in the bottom layers as layers add on later. Similarly, the longer hold times for the top most layers can be explained by the need for bringing the cure level from zero to the desired 90% quickly while those at the bottom continue to cure with attenuated UV during this time.

Figure 10 shows the evolution of the total robust optimal control input of UV intensity (feedforward plus feedback). For almost all layers except at the top most layers toward the end, the constructed feedback control law computed an additional (positive) UV intensity on top of the constant feedforward input of 100 mW/cm^2 . This can be explained by the final cure level result for the nominal optimal case (Case 2) shown in Fig. 6. For the worst case uncertainty considered, the final cure level reduces from the targeted one; as a result, the robust optimization computes a positive UV intensity to compensate for the cure level degradation in earlier layers to bring them to near complete cure.

Figure 11 shows the sensitivity of the final cure state with for two different values of the robustness measure β . For the considered uncertainty ($+10\%$ deviation in both E_2 and \bar{B}), by increasing the β value from 0.25 to 0.4, it can be seen that the sensitivity of the final cure state (across all layers) to the respective parameters is largely reduced. While there is still room for further improvement by increasing β , the nominal performance will deteriorate. The tradeoff between nominal performance and the risk due to uncertainty can also be examined by comparing the trends of cost function value plotted in Fig. 12, which shows the progress of the cost function during the computations of the optimization algorithm. As the cost component due to the sensitivity to parameter changes decreases, the nominal cost increases. This departure of the nominal cost from its optimal value will increase for higher values of the robustness measure β . For $\beta = 0.25$, the minimum total cost is achieved after 31 iterations.

5 Conclusion

This paper outlined a model-based robust optimization and control scheme for a layer-by-layer curing process for fabricating a thick polymer composite laminate. The paper first outlined experimental model verifications of a UV curing process model. Then, using a proposed hybrid systems modeling framework for the layer-by-layer process, the paper offered an inner and outer loop cascade control structure. At the outer loop, the layering times (the interlayer times) are posed as the control variables to be selected optimally via offline optimizations using the nominal model. Then, the closed-loop control of UV intensity with feedforward and output feedback is constructed to track a nominally optimal surface temperature trajectory. The static feedback gains at every mode or layer addition are optimized to compensate for performance degradation due to process uncertainty by defining the sensitivity of the objective function as a robustness measure and considering it as an additional cost function. The robust optimization problem is posed and solved by adjoining the corresponding system sensitivity and state dynamics within the hybrid framework.

The paper included simulation results for using the experimentally verified UV curing process model considering two uncertain parameters with significant effects on the cure dynamics: increase

in activation energy E_2 and decrease cure reaction constant \bar{B} . The simulations illustrated the advantages of the robust hybrid optimization schemes in achieving robust process performance via the augmented control inputs of open-loop nominal optimal-inter layer hold times and feedforward plus (optimal) feedback UV intensity in the presence of uncertain parameters.

Continuing investigations include development of an automated layering and control system that experimentally deploys the proposed schemes in a fully instrumented setting.

Acknowledgment

This research is supported, in part, by NSF under grant non-CMMI-1055254 and the U.S. Department of Energy's GATE Program DE-EE0005571.

References

- [1] Lucintel, 2010, "Growth Opportunities in Carbon Fiber Market 2010–2015," Irving, TX, http://www.lucintel.com/carbon_fiber_market.aspx.
- [2] Duan, Y., Li, J., Zhong, W., Maguire, R. G., Zhao, G., Xie, H., Li, D., and Lu, B., 2012, "Effects of Compaction and UV Exposure on Performance of Acrylate/Glass-Fiber Composites Cured Layer By Layer," *J. Appl. Polym. Sci.*, **123**(6), pp. 3799–3805.
- [3] Dufour, P., Michaud, D. J., Touré, Y., and Dhurjati, P. S., 2004, "A Partial Differential Equation Model Predictive Control Strategy: Application to Autoclave Composite Processing," *Comput. Chem. Eng.*, **28**(4), pp. 545–556.
- [4] Compston, P., Schiemer, J., and Cvetanovska, A., 2008, "Mechanical Properties and Styrene Emission Levels of a UV-Cured Glass-Fibre/Vinylester Composite," *Compos. Struct.*, **86**(1), pp. 22–26.
- [5] Beziers, D., Capdepuy, B., and Chataignier, E., 1990, *Electron Beam Curing of Composites*, Developments in the Science and Technology of Composite Materials, Springer, Dordrecht, The Netherlands, pp. 73–78.
- [6] Endrueit, A., Johnson, M. S., and Long, A. C., 2006, "Curing of Composite Components by Ultraviolet Radiation: A Review," *Polym. Compos.*, **27**(2), pp. 119–128.
- [7] Yebi, A., and Ayalew, B., 2015, "Partial Differential Equation-Based Process Control for Ultraviolet Curing of Thick Film Resins," *ASME J. Dyn. Syst. Meas. Control*, **137**(10), p. 101010.
- [8] Wang, X., 2001, "Modeling of In-Situ Laser Curing of Thermoset-Matrix Composites in Filament Winding," *Ph.D. Dissertation*, University of Nebraska, Lincoln, NE.
- [9] Wenbin, H., Tsui, L. Y., and Haiqing, G., 2005, "A Study of the Staircase Effect Induced by Material Shrinkage in Rapid Prototyping," *Rapid Prototyping J.*, **11**(2), pp. 82–89.
- [10] Yebi, A., and Ayalew, B., 2015, "Optimal Layering Time Control for Stepped-Concurrent Radiative Curing Process," *ASME J. Manuf. Sci. Eng.*, **137**(1), p. 011020.
- [11] Yebi, A., and Ayalew, B., 2015, "A Hybrid Modeling and Optimal Control Framework for Layer-By-Layer Manufacturing Process," American Control Conference Chicago, IL, pp. 3619–3624.
- [12] Yebi, A., and Ayalew, B., 2015, "A Hybrid Modeling and Robust Optimal Control for Layer-By-Layer Manufacturing Process," *IEEE Trans. Control Syst. Technol.*, **PP**(99), pp. 1–13.
- [13] Yebi, A., Ayalew, B., and Pilla, S., 2015, "Control-Oriented Model Verification for UV Processing of Composite Laminate," Society for the Advancement of Material and Process Engineering (SAMPE), Baltimore, MD.
- [14] Alamir, M., and Balloul, I., 1999, "Robust Constrained Control Algorithm for General Batch Processes," *Int. J. Control*, **72**(14), pp. 1271–1287.
- [15] Rustem, B., 1989, "Robust Optimal Policy Methods for Nonlinear Models," *IEEE 28th Conference on Decision and Control*, Tampa, FL, Dec. 13–15, pp. 2050–2055.
- [16] Darlington, J., Pantelides, C. C., Rustem, B., and Tanyi, B. A., 2000, "Decreasing the Sensitivity of Open-Loop Optimal Solutions in Decision Making Under Uncertainty," *Eur. J. Oper. Res.*, **121**(2), pp. 343–362.
- [17] Zhang, H., and James, M. R., 2006, " L_∞ Bounded Robust Control for Hybrid Systems," *IEEE 45th IEEE Conference on Decision and Control*, San Diego, CA, Dec. 13–15, pp. 4801–4806.
- [18] Nagy, Z. K., and Braatz, R. D., 2004, "Open-Loop and Closed-Loop Robust Optimal Control of Batch Processes Using Distributional and Worst-Case Analysis," *J. Process Control*, **14**(4), pp. 411–422.
- [19] Ruppen, D., Bonvin, D., and Rippin, D. W. T., 1998, "Implementation of Adaptive Optimal Operation for a Semi-Batch Reaction System," *Comput. Chem. Eng.*, **22**(1), pp. 185–199.
- [20] Srinivasan, B., and Bonvin, D., 2004, "Dynamic Optimization Under Uncertainty Via NCO Tracking: A Solution Model Approach," *BatchPro Symposium No. LA-CONF-2004-002*, Poros, Greece, June 6–9, pp. 17–35.
- [21] Podmajerský, M., and Fikar, M., 2009, "On-Line Neighbouring-Extremal Controller Design for Setpoint-Transition in Presence of Uncertainty," *17th International Conference on Process Control'09*, Štrbské Pleso, Slovak Republic, June 9–12, pp. 107–113.

- [22] Srinivasan, B., Bonvin, D., Visser, E., and Palanki, S., 2003, "Dynamic Optimization of Batch Processes II. Role of Measurements in Handling Uncertainty," *Comput. Chem. Eng.*, **27**(1), pp. 27–44.
- [23] Jiang, C., Teo, K. L., Loxton, R., and Duan, G.-R., 2012, "A Neighboring Extremal Solution for Optimal Switched Impulsive Control Problems With Large Perturbations," *Int. J. Innovative Comput., Inf. Control*, **8**(9), pp. 6235–6257.
- [24] Perry, M. F., and Young, G. W., 2005, "A Mathematical Model for Photopolymerization From a Stationary Laser Light Source," *Macromol. Theory Simul.*, **14**(1), pp. 26–39.
- [25] Yebi, A., Ayalew, B., and Dey, S., 2014, "Observer Design for State Estimation for UV Curing Process," *ASME Paper No. DSCC2014-6024*.
- [26] Bártolo, P., 2001, "Optical Approaches to Macroscopic and Microscopic Engineering," Ph.D. dissertation, University of Reading, Reading, UK.
- [27] Matias, J. M., Bartolo, P. J., and Pontes, A. V., 2009, "Modeling and Simulation of Photofabrication Processes Using Unsaturated Polyester Resins," *J. Appl. Polym. Sci.*, **114**(6), pp. 3673–3685.
- [28] Tang, Y., 2005, "Stereolithography Cure Process Modeling," Ph.D. Dissertation, *Georgia Institute of Technology*, Atlanta, GA.
- [29] Kim, W. S., Park, K. S., Nam, J. H., Shin, D., Jang, S., and Chung, T. Y., 2010, "Fast Cure Kinetics of a UV-Curable Resin for UV Nano-Imprint Lithography: Phenomenological Model Determination Based on Differential Photocalorimetry Results," *Thermochim. Acta*, **498**(1), pp. 117–123.
- [30] Voytekunas, V. Y., Ng, F. L., and Abadie, M. J. M., 2008, "Kinetics Study of the UV-Initiated Cationic Polymerization of Cycloaliphatic Diepoxide Resins," *Eur. Polym. J.*, **44**(11), pp. 3640–3649.
- [31] Gavin, H., 2011, "The Levenberg-Marquardt Method for Nonlinear Least Squares Curve-Fitting Problems," Department of Civil and Environmental Engineering, *Duke University*, Durham, NC, pp. 1–15.
- [32] Yebi, A., and Ayalew, B., 2016, "Model-Based Optimal Control of Layering Time for Layer-By-Layer UV Processing of Resin Infused Laminates," American Control Conference (ACC), Boston, MA, July 6–8.
- [33] Decker, C., 2001, "UV-Radiation Curing Chemistry," *Pigm. Resin Technol.*, **30**(5), pp. 278–286.